Aqueous Two-Phase System Formation Kinetics for Elastin-Like Polypeptides of Varying Chain Length

Yanjie Zhang, Kimberly Trabbic-Carlson, Fernando Albertorio, Ashutosh Chilkoti, and Paul S. Cremer*

Department of Chemistry, Texas A&M University, 3255 TAMU, College Station, Texas 77843, and Department of Biomedical Engineering, Duke University, Durham, North Carolina 27708

Received March 18, 2006; Revised Manuscript Received May 1, 2006

The kinetics of aqueous two-phase system (ATPS) formation for elastin-like polypeptides (ELP) with defined chemical composition and chain length was investigated by dark field microscopy in an on-chip format with a linear temperature gradient. Scattering intensities from peptide solutions in the presence and absence of sodium dodecyl sulfate (SDS) were recorded as a function of temperature and time, simultaneously. It was found that the formation of the ATPS for three ELPs of different molecular weights (36 075, 59 422, and 129 856 Da) in the absence of SDS followed a coalescence mechanism, and the rate constant and activation energy were independent of chain length. With the introduction of SDS into the ELP solutions, the rate constants were attenuated more strongly with increasing chain length. Moreover, the coalescence process in the presence of SDS showed non-Arrhenius kinetics as a function of temperature. For the two shorter ELPs, ATPS formation occurred via coalescence at all SDS concentrations and temperatures investigated. On the other hand, the coalescence process was greatly suppressed for the longest ELP at elevated temperatures and higher SDS concentrations. Under these circumstances, ATPS formation was forced to proceed via a mixed Ostwald ripening and coalescence mechanism.

Introduction

The formation of an aqueous two-phase system[1−3] commences when a macromolecular system spontaneously separates into two separate water-containing phases. Such phenomena often involve two polymers separating into distinct phases with different densities. ATPS formation may also occur in solutions consisting of a single polymer plus a high concentration of an appropriate salt[4−7] or even in the absence of salt for certain thermoresponsive polymers.[8−10] In this final case, ATPS formation occurs above the polymer's lower critical solution temperature (LCST). For these systems, a denser polymer-rich phase is formed on the bottom of the container, while the upper phase consists primarily of pure water. Since the phase boundary in an ATPS has very low interfacial tension,[11] these systems have been widely applied as tools for bioseparations without significant interfacial denaturing effects.[12−14]

Despite the practical and fundamental significance of ATPS formation, there is almost no literature dealing with its formation kinetics because of the difficulties involved in data collection. To remedy this problem, we recently developed a temperature-gradient microfluidic technique[15−17] that allows ATPS formation to be followed in a high-throughput, low sample volume fashion.[18] This enabled us to explore the activation energy of the process for α-elastin, a thermoresponsive protein, which was prepared by the methods of Partridge et al.[19] It was found that there are two major mechanistic pathways through which ATPS formation could proceed: coalescence and Ostwald ripening. Coalescence is the direct fusion of one particle with another to make a larger one, while Ostwald ripening involves the growth of particles through the transfer of individual molecules between them such that bigger particles grow at the expense of smaller ones.[20] Each process has a different activation barrier associated with it. In the case of coalescence, the barrier comes from the removal of intervening solvent molecules between the particles which are being joined. On the other hand, Ostwald ripening involves the desorption of single macromolecules from shrinking particles and their deposition onto growing particles. The rate constants of ATPS formation for elastin are consistent with a coalescence mechanism, although the process can be forced to proceed through Ostwald ripening by the addition of sodium dodecyl sulfate to the solution.

We suspected that the mechanism of ATPS formation might be dependent on the molecular weight of the polymer; however, the natural product, α-elastin, is a mixture of cross-linked materials that is highly polydisperse. Therefore, to obtain more control over the molecular weight, we employed elastin-like polypeptides. ELPs are based on a repetitive pentapeptide motif, Val-Pro-Gly-Xaa-Gly, where the guest residue, Xaa, is any amino acid except Pro. The sequence and chain length can be precisely controlled by genetic expression in bacteria using recombinant DNA techniques.[21,22] The work described herein was undertaken with three different molecular weight species (36 075, 59 422, and 129 856 Da) to investigate the effect of chain length on the kinetics of ATPS formation. It was found that coalescence in the absence of SDS is not dependent on the chain length of the ELPs; however, SDS increases the activation barrier for the coalescence process of longer-chain ELPs to a greater extent than for shorter ones. In fact, the ATPS formation process could be forced to go by Ostwald ripening at higher temperatures and SDS concentrations in the case of the 129 856 Da ELP, but not for the two smaller molecules.

Experimental Section

The ELPs employed herein come from a library of ELP[$V_5A_2G_3$-*n*] where the repeat sequence of amino acids is the same. Members within the library differ only in their chain length, where *n* is the number of pentapeptides. For example, ELP[$V_5A_2G_3$-90] consists of 90 pentapeptides and has a repeat unit composed of 10 pentapeptides with the guest

10.1021/bm060254y CCC: $33.50
Published on Web 06/20/2006

residues Val, Ala, and Gly in a 5:2:3 ratio. Since only this one chemistry was employed in the experiments below, the notation for the ELPs is simplified to ELP-90 (36 075 Da), ELP-150 (59 422 Da), and ELP-330 (~129 856 Da).

Low-conductivity H_2O, produced from a NANOpure Ultrapure Water System (Barnstead, Dubuque, IA) with a minimum resistivity of 18 MΩ·cm, was used to prepare sodium phosphate buffer solutions (10 mM, pH = 7.0). Sodium dodecyl sulfate was obtained from Fluka. ELPs were dissolved in the buffer at concentrations of 13.3 mg/mL with various concentrations of SDS. It should be noted that we always kept the concentration of SDS well below its critical micelle concentration (cmc), which is about 8.1 mM near room temperature in polymer-free solution.[23]

ATPS kinetics was followed using a temperature-gradient apparatus placed on a dark field microscope. The fabrication of the temperature-gradient device has been described previously.[15−18] Briefly, a cover glass acting as a sample stage and heat conductor was mounted on top of two parallel brass tubes ($^1/_8$ in wide, K & S Engineering, Chicago, IL), through which hot and cold antifreeze solutions could be individually flowed using standard water bath circulators (Fisher Scientific, Pittsburgh, PA). Rectangular borosilicate capillary tubes (VitroCom, Inc.) with dimensions of 2 cm × 1 mm × 100 μm (length × width × height) were used as sample containers and placed parallel to the temperature gradient. Light scattering from the peptide solutions was monitored via a CCD camera (Micromax 1024, Princeton Instruments) using dark field optics under an inverted microscope (Nikon, TE2000-U). Two different polymer solutions with previously measured LCSTs served to calibrate the slope of the gradient for each experiment.[16−18] The first solution was 10 mg/mL poly(*N*-isopropylacrylamide) in H_2O with a known LCST of 30.2 ± 0.1 °C, and the second was 10 mg/mL poly(*N*-isopropylacrylamide) in a 0.7 M KCl solution with a known LCST of 26.0 ± 0.1 °C. Six rectangular capillary tubes could be fit side-by-side under a 2× objective, and time-lapse CCD images were taken every 5 s to follow the kinetics of ATPS formation. The temperature along the capillary tubes could be determined by counting the pixels in a linescan drawn along the temperature gradient in the CCD images.

Diameters of the ELP particles as a function of SDS concentration were measured by dynamic light scattering (DLS) using a Brookhaven Instruments 90Plus particle size analyzer at a 90° scattering angle and 25 °C. The light source was a 35 mW diode laser at 632.0 nm. To measure the mean diameter of the particles formed in ELP solutions, the autocorrelation functions were analyzed by ZetaPlus Particle Sizing Software version 3.46.

Results

LCST of ELPs. In a first set of experiments, the LCSTs of ELP-90, ELP-150, and ELP-330 were measured with varying SDS concentrations under a dark field microscope. The initial images were captured within a few seconds of placing the samples on the temperature gradient. A line scan was drawn parallel to the temperature gradient across each sample, and the onset point for the LCST of each ELP is plotted as a function of SDS concentration in Figure 1. As can be seen from the data, the LCST decreased with increasing molecular weight of the macromolecules. This result is in good agreement with previous studies performed in the absence of SDS.[21,22] The LCSTs of all three ELPs initially decreased at low SDS concentration but then began to rise with increasing SDS concentration. This behavior is reminiscent of the effects observed for sodium *n*-alkyl sulfates with $n = 5-8$ on the LCST of poly(*N*-isopropylacrylamide).[24] The initial depression of the LCST is likely caused by hydrophobic interactions between the SDS and the polymer. It is known that small hydrophobic alcohols such as *n*-butanol give rise to similar salting-out effects at all

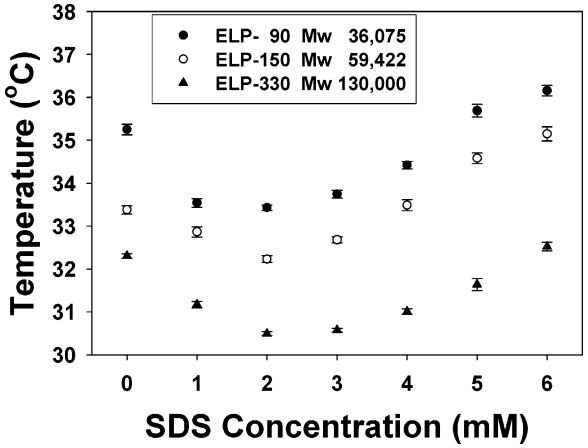

Figure 1. LCST values of ELPs with different molecular weights as a function of SDS concentration.

concentrations.[25] At higher concentrations, however, the SDS molecules sufficiently coat the ELP to form polymer-bound micelles. This coating should decrease the surface tension of the polymer/aqueous interface. Furthermore, the electrostatic repulsion between charged polymer-bound micelles will also come into play.[24] This combination of electrostatic repulsion and a lowering of the surface tension for the ELP molecules should impede collapse and aggregation of the particles. In fact, previous studies have shown that SDS tends to prevent intermolecular aggregation of the polymer chains.[26]

The model described above was further tested by dynamic light scattering measurements at varying SDS concentrations for the three ELPs at a temperature just below the onset of the LCST, 25 °C (Figure 2). As expected, the ELPs tend to form aggregates in the absence of SDS. The change in mean aggregate size closely tracked changes in the LCST value as SDS was added. Low concentrations of SDS showed little or no effect on the particle size. In the case of ELP-330, a small increase in mean particle size could actually be noted by the addition of 2 mM SDS. At higher SDS concentrations, the mean particle size dropped dramatically for all three ELPs.

ATPS Formation in the Absence of SDS. Under the conditions of these experiments, ATPS formation took place over the course of several hundred seconds as evidenced by a decrease in scattering intensity of the precipitated ELPs with time. The end point of ATPS formation was judged to have occurred once no significant scattering from the ELP solutions could be detected. The entire process was recorded by a time-lapse image series. A three-dimensional plot of the light scattering intensity versus temperature and time for 13.3 mg/mL ELP-150 in 10 mM phosphate buffer is shown in Figure 3a as an example. At any given temperature, the decay of the scattering intensity as a function of time could be fit by a single-exponential decay function (eq 1)

$$y = y_0 + a\,e^{-kt} \tag{1}$$

where y is the intensity of the scattered light, y_0 is the background intensity, a is a proportionality factor, k is the rate constant for the process, and t is time. A sample curve from this data set at 40.0 °C is shown in Figure 3b. By fitting the data, the rate constants of ATPS formation for ELPs with different chain lengths could be determined as a function of temperature (Figure 3c). It was readily observable that k values increased with increasing temperature, and they were quite similar for different chain lengths at a given temperature. The temperature dependence of the rate constant could be expressed

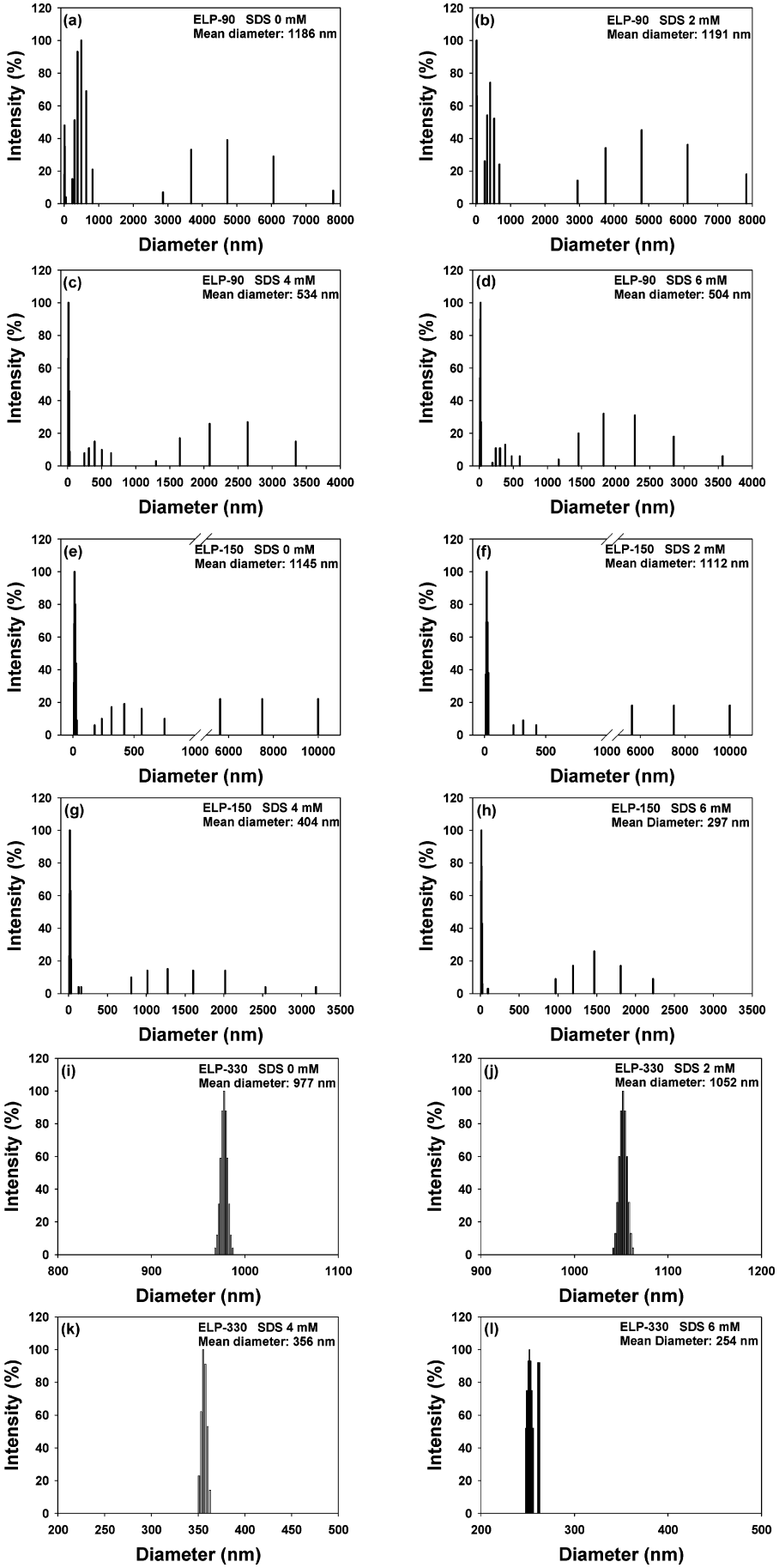

Figure 2. Particle size distributions for 13.3 mg/mL ELP solutions at 25 °C with varying SDS concentration. The molecular weight of the ELP and the concentration of SDS are indicated on each plot.

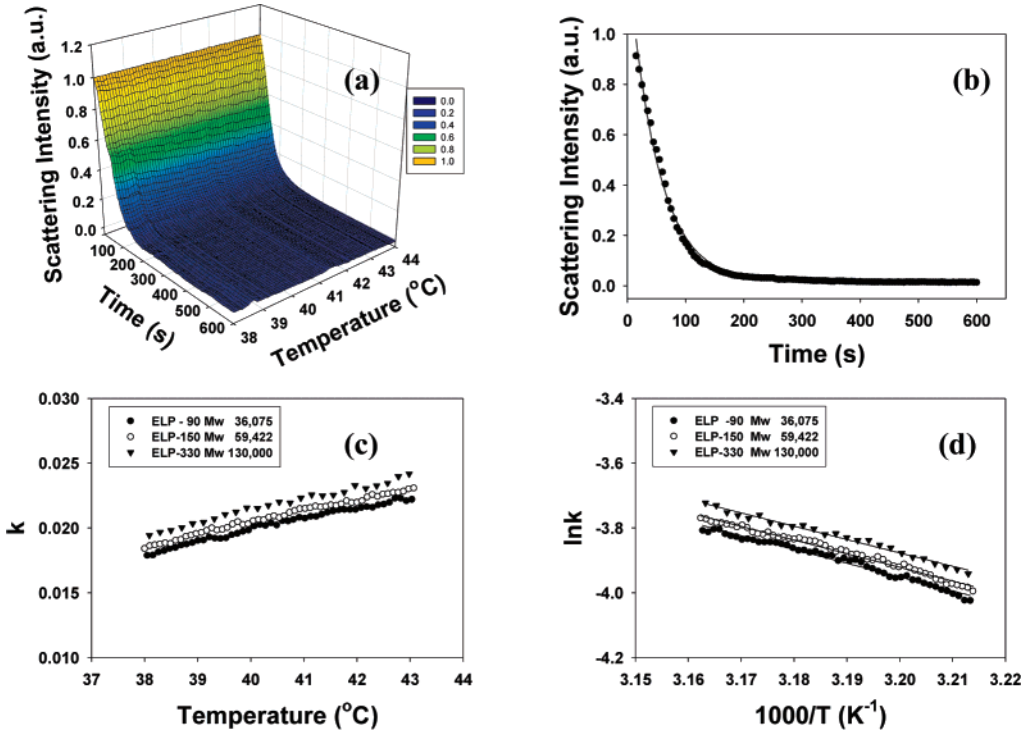

Figure 3. (a) A three-dimensional plot of light scattering intensity versus time and temperature of a 13.3 mg/mL ELP-150 solution. (b) A curve fit to data in (a) by eq 1 at 40.0 °C. (c) The rate constant, *k*, for ATPS formation of ELPs with different molecular weights as a function of temperature. (d) Arrhenius plots of the data from (c).

by the Arrhenius equation

$$k = A \exp(-\Delta E/RT) \qquad (2)$$

where A is a prefactor, R is the gas constant, ΔE is the apparent activation energy, and T is the temperature in Kelvin. A plot of $\ln(k)$ versus $1/T$ for these data is shown in Figure 3d. ΔE can be obtained from the slope of the linear regression curve. The value of ΔE was 8.4 ± 0.5 kcal/mol regardless of the chain length of the ELP. Such first-order kinetics is consistent with ATPS formation via a coalescence process, which is analogous to the behavior of α-elastin in phosphate buffer.[18] In fact, the values for the activation energy are almost identical to those of coalescing α-elastin.[18]

ATPS Formation in the Presence of SDS. The introduction of SDS to the ELP solutions suppressed the rate constant for ATPS formation. Figure 4a shows the rate constant of coalescence obtained by fitting with eq 1 for ELP-90 at various SDS concentrations. At low surfactant concentrations, the rate constant dropped only at elevated temperatures, but at sufficient SDS concentrations, the rate decreased over the entire temperature range investigated. The effect of SDS on ELP-150 was qualitatively similar to that for ELP-90 (Figure 4b), but more pronounced. Indeed, similar SDS concentrations already led to a drop in the rate at lower temperatures for the longer polypeptide. Although SDS lowered the rate constant of coalescence, the decay of light scattering intensity with time still could be well-fit by eq 1, and ATPS formation appeared to go to completion.[27] The three-dimensional plots for scattering intensity vs time and temperature for ELP-90 and ELP-150 at various SDS concentrations look very similar to each other and are consistent with a coalescence mechanism in both cases (data not shown). Unfortunately, however, the decrease in rate constants with temperature made it impossible to obtain activation barriers using standard Arrhenius analysis (Figure 4c,d).

For the longest ELP chain length investigated, ELP-330, the addition of SDS into the peptide solution changed the ATPS formation process dramatically even at low concentration. Figure 5 shows the three-dimensional plots of light scattering intensity versus time and temperature at SDS concentrations of (a) 0 mM, (b) 0.6 mM, (c) 1.4 mM, and (d) 1.8 mM, respectively. The decay of scattering intensity with time is clearly slowed by the addition of SDS at high temperature and SDS concentration. This phenomenon was observable from the 3-D plots when the SDS concentration reached 0.6 mM and was more pronounced at 1.4 mM. At 1.8 mM SDS, the ATPS formation rate was inhibited from coming to completion at sufficiently high temperature (Figure 5d).

In contrast to ELP-90 and ELP-150, very low SDS concentrations caused drastic changes in the rate constant of ATPS formation for ELP-330, and the process could not be fit by first-order kinetics at higher temperatures for those SDS concentrations above 1.0 mM. For the ELP-330 solution containing 1.8 mM SDS, the rate of ATPS formation decreased dramatically compared to the same solution without SDS and did not follow first-order kinetics at higher temperatures. Figure 6a shows the scattering intensity of an ELP-330 solution with 1.8 mM SDS as a function of time at different temperatures. From Figure 6a, it can be readily seen that the shape of the curves changed gradually between 35.1 and 43.1 °C. At the lowest temperatures, the fit to eq 1 (first-order kinetics) was excellent, while it became increasingly poor as the temperature was increased.

Figure 6b plots the reciprocal of scattering intensity vs time for temperatures between 40.1 and 43.1 °C. The idea for plotting the high-temperature data in this fashion was to determine whether the scattering intensity attenuation followed the equation for second-order kinetics, which is consistent with Ostwald ripening

$$\frac{1}{y} = kt + C \qquad (3)$$

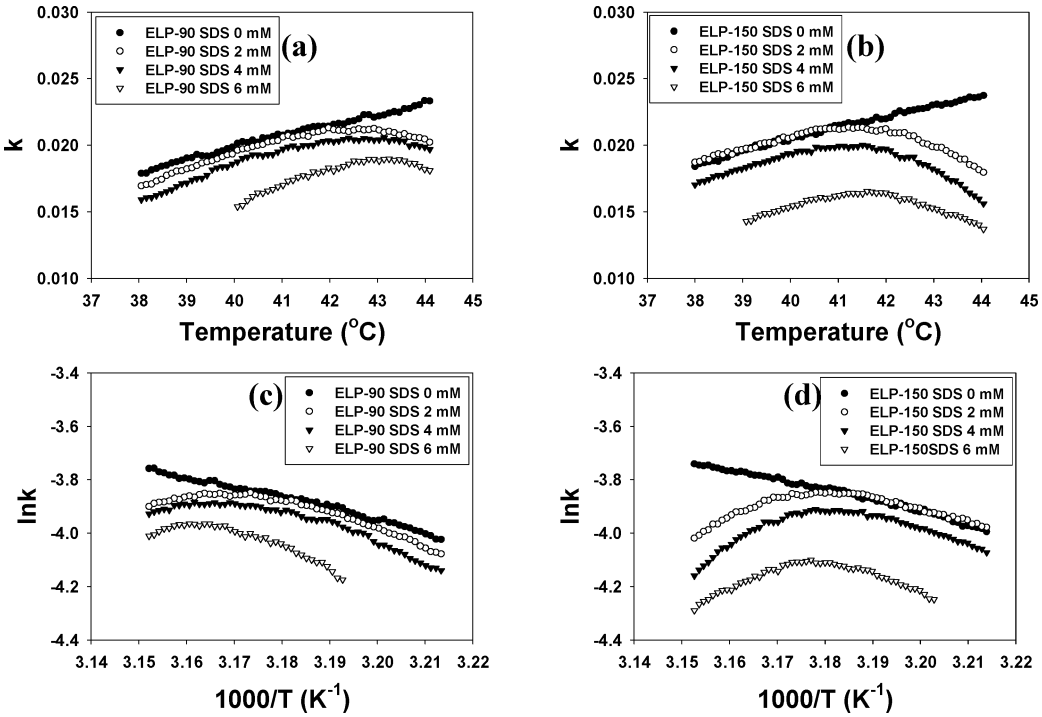

Figure 4. The rate constant, *k*, for ATPS formation at different SDS concentrations as a function of temperature for (a) ELP-90 and (b) ELP-150. The data for (c) ELP-90 and (d) ELP-150 are replotted as ln(*k*) vs 1/*T*. All *k* values were obtained by employing eq 1.

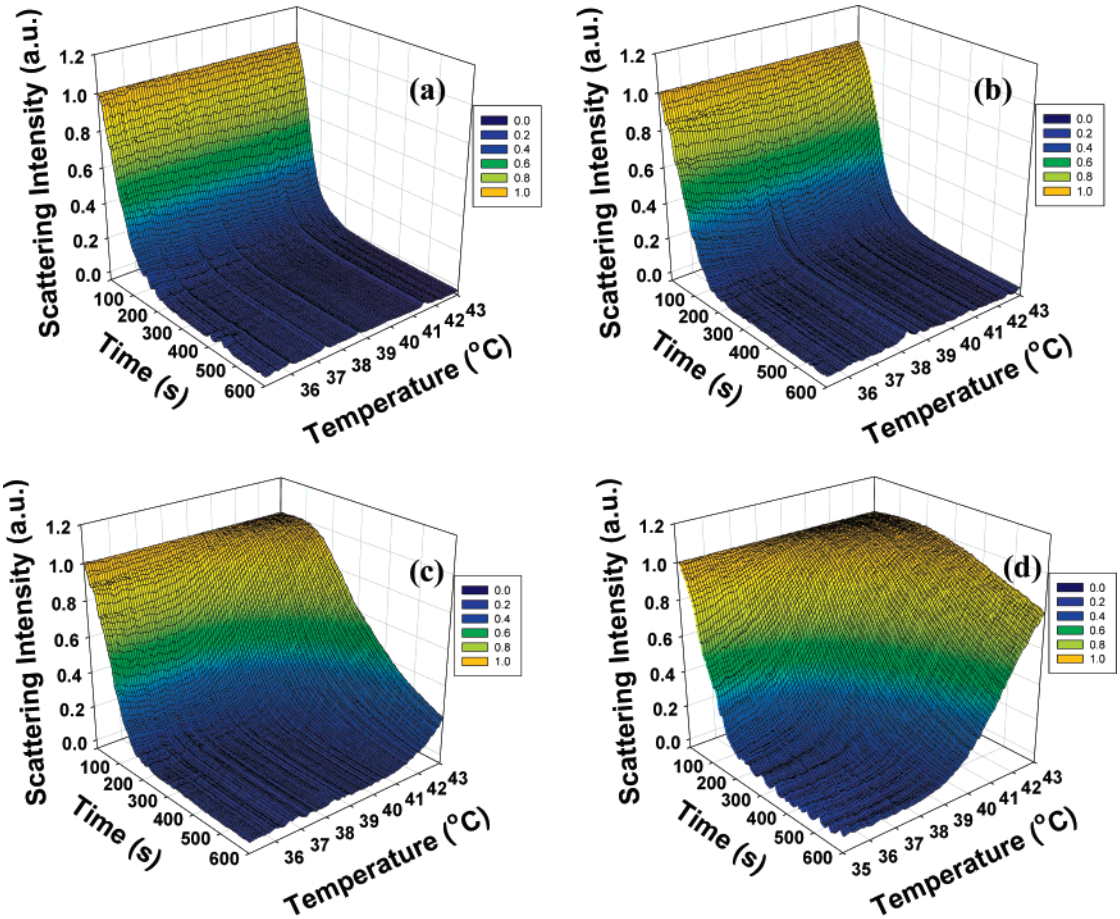

Figure 5. Three-dimensional plots of light scattering intensity versus time and temperature of a 13.3 mg/mL ELP-330 solution at different SDS concentrations: (a) 0 mM; (b) 0.6 mM; (c) 1.4 mM; (d) 1.8 mM.

Here, *y* stands for the light scattering intensity, *C* is a constant which represents the reciprocal of the scattering intensity at the onset of ATPS formation, *k* is the rate constant, and *t* is time. As can be seen, the data at 43.1 °C (see insert) fit this equation better than the data near 40.1 °C, which were more highly curved. However, none of the data could be categorized as

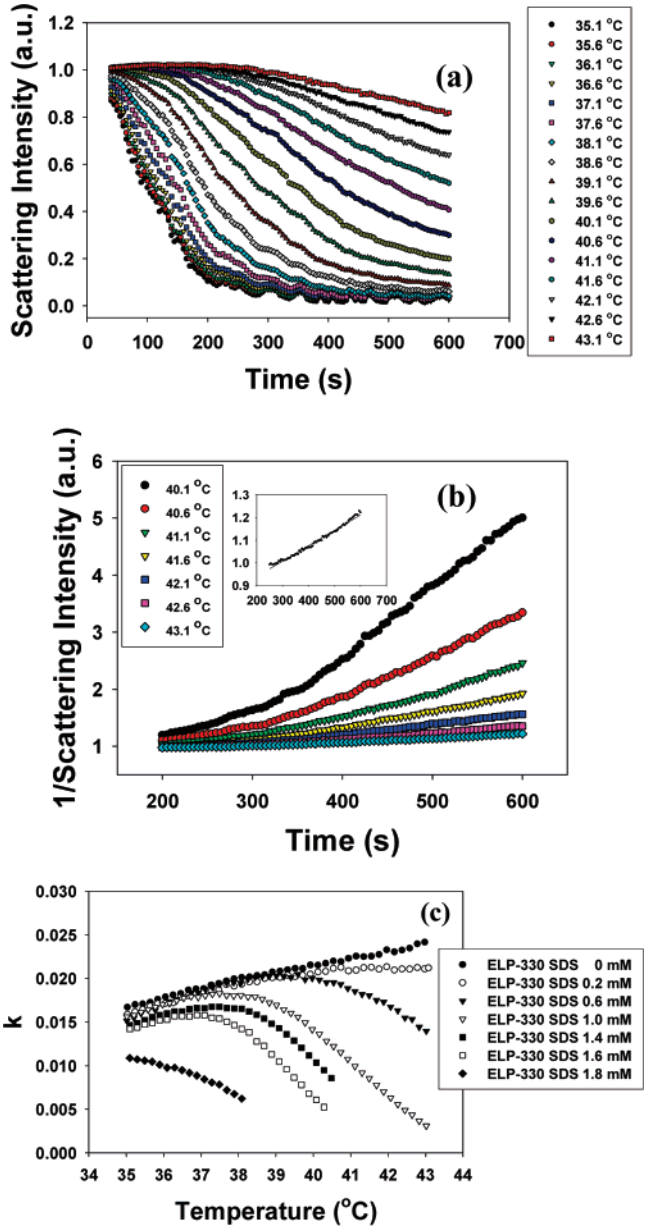

Figure 6. (a) Light scattering intensity of a 13.3 mg/mL solution of ELP-330 with 1.8 mM SDS at various temperatures as a function of time. (b) Reciprocal plot of scattering intensity vs time for ELP-330 with 1.8 mM SDS at various temperatures. The inset shows a blowup of the *y*-axis for data taken at 43.1 °C. (c) The rate constant, *k*, obtained from first-order kinetics of ELP-330 at different SDS concentrations as a function of temperature.

obeying purely second-order kinetics. Indeed, the data represented a mixture of first- and second-order kinetics. However, as the temperature was elevated, the fit to a second-order equation became better. This suggested that the ATPS formation process for ELP-330 followed a coalescence mechanism at low temperature, but continuously changed over to Ostwald ripening with increasing temperature.

Another illustration of the turning off of the coalescence mechanism for ELP-330 is shown in Figure 6c. In this case, data at lower temperatures and SDS concentrations are fit to eq 1. As can be seen, the *k* versus *T* plots were already curved for 0.2 mM SDS at higher temperatures. Furthermore, even lower temperature data showed nonlinear behavior in the presence of 1.8 mM SDS, and data above 38.1 °C needed to be omitted, as they were impossible to fit by first-order kinetics.

ATPS as a Function of ELP Concentration in the Presence of SDS. It should be noted that all the experiments described above were conducted with 13.3 mg/mL of the respective ELPs. Therefore, the concentration of monomer was the same in each system, but the concentration of polymer chains varied. In fact, the molar concentration of ELP-90 was 0.37 mM, while the concentrations of ELP-150 and ELP-330 were 0.22, and 0.10 mM, respectively. Therefore, the changes in mechanism for the largest ELP could have been caused by changes in molar concentration as well as molecular weight. Several control experiments emphasized the importance of molecular weight effects (data not shown). For example, a control experiment was performed with 29 mg/mL ELP-330, which matches the molar concentration of ELP-150 at 13.3 mg/mL. In this case, ELP-330 showed the same change in mechanism from one dominated by coalescence to one dominated by Ostwald ripening. This change occurred at somewhat higher SDS concentration (6 mM) than was the case for 0.10 mM ELP-330 (1.8 mM). However, ELP-150 showed no tendency to switch to an Oswald ripening mechanism for ATPS formation at 6 mM SDS and 0.22 mM ELP.

Discussion

ELPs undergo reversible phase transitions in aqueous solutions above their LCST.[28−30] The peptides form coacervate droplets above the transition temperature due to the collapse and aggregation of peptide molecules.[31] Upon standing, the suspension clears with the formation of the ATPS. It is generally thought that in undisturbed solutions the coarsening of particles follows a coalescence mechanism if the interfacial tension is reasonably high.[32] On the other hand, Ostwald ripening contributes in systems with sufficiently low interfacial tension. The coalescence of droplets is an activated process which involves the removal of the interfacial solvent film between two particles.[33] The kinetics of the process is closely related to the interfacial tension between the particles and the solvent.[34]

For the ELPs used in the present studies, the chemical structures were identical, but the chain lengths of the polymers varied. The interfacial tension between ELP particles and water in the absence of SDS for different chain lengths was identical as evidenced by the rate constants and activation energies obtained. The simple ATPS formation process for ELPs without SDS is illustrated in the top line of Figure 7.

When SDS is added to an ELP solution, hydrophobic association can occur between the surfactant and the peptide.[35] When the temperature is higher than the LCST, the ELP undergoes hydrophobic collapse, and the SDS molecules are presumably expelled from the inside of nascently formed polypeptide aggregates and forced to adsorb onto their surfaces instead (Figure 7).[23,36] It has been previously shown that the introduction of sodium dodecyl sulfate decreases the interfacial tension[20] between ELP particles and lowers the rate of coalescence.[18,34] On the basis of the results described in Figures 3−6, it is clear that ATPS formation proceeds in a molecular weight dependent fashion when SDS is introduced to the system.

Molecular weight dependent interactions with SDS have been found for a variety of aqueous polymer systems including poly(ethylene glycol),[37−39] poly(vinylpyrrolidone),[40,41] hydrophobic ethoxylated urethane,[42] and cationic hydroxyethyl cellulose.[43] In those cases, it was generally found that surfactant−polymer interactions were weak at low molecular weight, became increasingly strong as the polymer chain was lengthened, and eventually became molecular weight independent above a

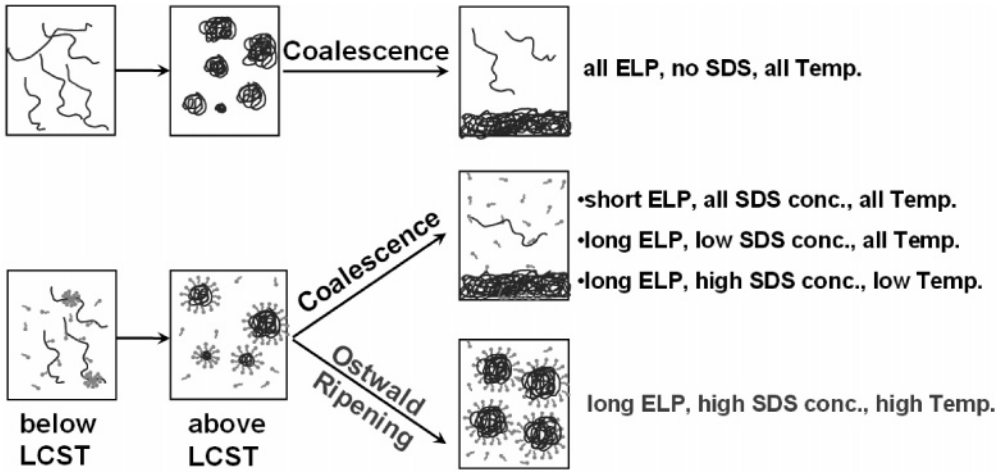

Figure 7. Schematic diagram of the ATPS formation process for ELPs with different chain lengths in the presence and absence of SDS.

threshold value.[37−39,44] Such results have been interpreted as an increase in the apparent hydrophobicity of the polymer as the chain length increases,[38] which allows for more favorable interactions with SDS molecules.[45,46] Despite a variety of surface tension,[37] conductivity,[37] NMR,[39] photoluminescence probe,[40] and isothermal calorimetry (ITC) studies,[38,39,42] the mechanism for this phenomenon remains a matter of debate. The interactions are, however, generally believed to be complex. For example, both endothermic and exothermic interactions have been found by ITC.[38,39,42] Furthermore, ion−dipole as well as hydrophobic interactions have been proposed to explain the process.[38,39,42]

In the present system, the rate constants for coalescence of ELP-330 solutions are decreased dramatically in the presence of SDS at fairly low concentrations compared to those for ELP-90 and ELP-150 (Figures 3 and 5). Such a result is consistent with the idea that the activation barrier to coalescence is raised dramatically as a function of chain length. This in turn explains why only the longest ELP undergoes ATPS formation via Ostwald ripening rather than the shorter molecules in the presence of SDS. In fact, one would have expected to find the opposite result if the barrier to coalescence were not affected by the polymer chain length in the presence of SDS.[47−49] Indeed, if the barrier to coalescence were sufficiently high for all chain lengths, then all of the ELP systems would be forced to undergo ATPS formation via Ostwald ripening. As noted above, this process involves the removal of single macromolecules from shrinking particles and the addition of these polymer chains to growing particles. Therefore, a multivalency effect might be expected, whereby the activation barrier to chain removal would go up with chain length. This effect is probably obscured here by the chain length dependence of the activation barrier to coalescence. Although performing experiments with longer chain length ELPs might help resolve this issue, they are very difficult to synthesize using current technology.[21,22]

A final issue that needs to be addressed is the non-Arrhenius kinetics of the coalescence rate constants for the ELP−SDS systems. Figures 4 and 6c clearly show that the rate constant first increases with temperature, but then decreases sharply. Previously, analogous non-Arrhenius kinetics have been observed for protein folding[50,51] and loop closure of DNA hairpins.[52] This behavior was closely related to the temperature dependence of the hydrophobic effect.[53] At high temperatures, ELP molecules are more dehydrated than at low temperature; thus, the hydrophobic interactions between an ELP particle and SDS will be enhanced. This increased interaction as the temperature is raised should cause the ELP chains to be more completely coated with SDS for a fixed set of concentration conditions. Consequently, the barrier to coalescence should increase as the temperature is raised. In the case of ELP-90 and ELP-150, this only caused a decrease in the rate of ATPS formation, but the dominant reaction mechanism was still a coalescence process, as all data could be fit by first-order kinetics. In the case of ELP-330, however, the activation barrier to coalescence was finally elevated sufficiently in the presence of 1.8 mM SDS and temperatures exceeding 38.1 °C that the dominant mechanism for ATPS formation began to shift to Ostwald ripening. The evidence for this is clearly shown in Figure 5d. Ostwald ripening tended to make the size of the particles in the solution uniform and proceeded ever more slowly with increasing particle size.[54] The lack of completion of the ATPS process can be considered the hallmark of an event that is dominated by Ostwald ripening.[18] A schematic drawing of this final pathway is presented on the bottom of Figure 7.

Conclusions

The results reported in this paper describe the kinetics of ATPS formation for ELPs with defined chemical composition and chain length in the presence and absence of SDS. The following conclusions about the mechanism of ATPS formation for ELPs can be drawn: (1) In the absence of SDS, ATPS formation followed a coalescence pathway, and the rate constants and activation energy of this process were independent of the chain length of the ELP. (2) The coalescence of ELP particles in the absence of SDS showed Arrhenius kinetics as a function of temperature. (3) In the presence of SDS, there is a chain length dependence for coating ELPs with surfactant; and at sufficient chain lengths, SDS concentrations, and temperatures, the ATPS formation process is forced to proceed via Ostwald ripening. (4) The coalescence process for ELPs in the presence of SDS exhibits non-Arrhenius kinetics as a function of temperature, which is most likely related to the temperature dependence of the hydrophobic interactions between ELPs and SDS.

Acknowledgment. P.S.C. thanks the Army Research Office DAAD19-01-1-0346 and the Robert A. Welch Foundation (grant A-1421) for funding. A.C. acknowledges the financial support of the National Institutes of Health through grants 5R01-EB-000188 and 2R01-GM-61232. Additional support came from a Beckman Young Investigator Award, an Alfred P. Sloan Fellowship, and a Camille Dreyfus Teacher Scholar Award (P.S.C.).

References and Notes

(1) Sinha, J.; Dey, P. K.; Panda, T. *Appl. Microbiol. Biotechnol.* **2000**, *54*, 476−486.
(2) Hatti-Kaul, R. *Mol. Biotechnol.* **2001**, *19*, 269−277.
(3) Hatti-Kaul, R. In *Aqueous Two-Phase Systems. Methods and Protocols*; *Methods in Biotechnology*; Humana Press: Totowa, New Jersey, 2000; Vol. 11, pp 1−10.
(4) Albertsson, P.-A. *Partition of cell particles and macromolecules*; 3rd ed.; Wiley: New York, 1986.
(5) Ban, T.; Shibata, M.; Kawaizumi, F.; Nii, S.; Takahashi, K. *J. Chromatogr., B* **2001**, *760*, 65−72.
(6) Merchuk, J. C.; Andrews, B. A.; Asenjo, J. A. *J. Chromatogr., B* **1998**, *711*, 285−293.
(7) Baxter, S. M.; Sperry, P. R.; Fu, Z. W. *Langmuir* **1997**, *13*, 3948−3952.
(8) Johansson, H. O.; Karlström, G.; Tjerneld, F. *Macromolecules* **1993**, *26*, 4478−4483.
(9) Johansson, H. O.; Karlström, G.; Tjerneld, F. *Biochim. Biophys. Acta* **1997**, *1335*, 315−325.
(10) Johansson, H. O.; Persson, J.; Tjerneld, F. *Biotechnol. Bioeng.* **1999**, *66*, 247−257.
(11) Jiang, J. W.; Prausnitz, J. M. *J. Phys. Chem. B* **2000**, *104*, 7197−7205.
(12) Water, H.; Johansson, G. *Methods Enzymol.* **1994**, *228*.
(13) Persson, J.; Nyström, L.; Ageland, H.; Tjerneld, F. *J. Chromatogr., B* **1998**, *711*, 97−109.
(14) Li, M.; Zhu, Z. Q.; Rodrigues, A. E. *Ind. Eng. Chem. Res.* **2002**, *41*, 251−256.
(15) Mao, H. B.; Yang, T. L.; Cremer, P. S. *J. Am. Chem. Soc.* **2002**, *124*, 4432−4435.
(16) Mao, H. B.; Li, C. M.; Zhang, Y. J.; Bergbreiter, D. E.; Cremer, P. S. *J. Am. Chem. Soc.* **2003**, *125*, 2850−2851.
(17) Mao, H. B.; Li, C. M.; Zhang, Y. J.; Furyk, S.; Cremer, P. S.; Bergbreiter, D. E. *Macromolecules* **2004**, *37*, 1031−1036.
(18) Zhang, Y. J.; Mao, H. B.; Cremer, P. S. *J. Am. Chem. Soc.* **2003**, *125*, 15630−15635.
(19) Partridge, S. M.; Davis, H. F.; Adair, G. S. *Biochem. J.* **1955**, *61*, 11−21.
(20) Taylor, P. *Adv. Colloid Interface Sci.* **1998**, *75*, 107−163.
(21) Meyer, D. E.; Chilkoti, A. *Biomacromolecules* **2002**, *3*, 357−367.
(22) Meyer, D. E.; Chilkoti, A. *Biomacromolecules* **2004**, *5*, 846−851.
(23) Walter, R.; Rička, J.; Quellet, C.; Nyffenegger, R.; Binkert, T. *Macromolecules* **1996**, *29*, 4019−4028.
(24) Schild, H. G.; Tirrell, D. A. *Langmuir* **1991**, *7*, 665−671.
(25) Louai, A.; Sarazin, D.; Pollet, G.; Francois, J.; Moreaux, F. *Polymer* **1991**, *32*, 713−720.
(26) Dhara, D.; Chatterji, P. R. *J. Macromol. Sci., Rev. Macromol. Chem. Phys.* **2000**, *C40*, 51−68.
(27) It should be noted that under certain conditions the polypeptide structure may continue to mature in the protein-rich phase after the ATPS is formed. Such a process, however, was not directly observed in our assays.
(28) Urry, D. W. *Methods Enzymol.* **1982**, *82*, 673−717.
(29) Urry, D. W. *Angew. Chem., Int. Ed. Eng.* **1993**, *32*, 819−841.
(30) Urry, D. W. *J. Phys. Chem. B* **1997**, *101*, 11007−11028.
(31) Kaibara, K.; Watanabe, T.; Miyakawa, K. *Biopolymers* **2000**, *53*, 369−379.
(32) Fortelný, I.; Živný, A.; Jůza, J. *J. Polym. Sci., Part B: Polym. Phys.* **1999**, *37*, 181−187.
(33) Lyu, S. *Macromolecules* **2003**, *36*, 10052−10055.
(34) Dobler, F.; Pith, T.; Lambla, M.; Holl, Y. *J. Colloid Interface Sci.* **1992**, *152*, 1−11.
(35) Cooper-White, J. J.; Crooks, R. C.; Chockalingam, K.; Boger, D. V. *Ind. Eng. Chem. Res.* **2002**, *41*, 6443−6459.
(36) Zhu, P. W.; Napper, D. H. *Langmuir* **1996**, *12*, 5992−5998.
(37) Schwuger, M. J. *J. Colloid Interface Sci.* **1973**, *43*, 491−498.
(38) Dai, S.; Tam, K. C. *J. Phys. Chem. B* **2001**, *105*, 10759−10763.
(39) Bernazzani, L.; Borsacchi, S.; Catalano, D.; Gianni, P.; Mollica, V.; Vitelli, M.; Asaro, F.; Feruglio, L. *J. Phys. Chem. B* **2004**, *108*, 8960−8969.
(40) Turro, N. J.; Baretz, B. H.; Kuo, P.-L. *Macromolecules* **1984**, *17*, 1321−1324.
(41) Sesta, B.; D'Aprano, A.; Segre, A. L.; Proietti, N. *Langmuir* **1997**, *13*, 6612−6617.
(42) Dai, S.; Tam, K. C.; Wyn-Jones, E.; Jenkins, R. D. *J. Phys. Chem. B* **2004**, *108*, 4979−4988.
(43) Zhou, S.; Xu, C.; Wang, J.; Golas, P.; Batteas, J. *Langmuir* **2004**, *20*, 8482−8489.
(44) Goddard, E. D. *Colloids Surf.* **1986**, *19*, 255−300.
(45) Singh, S. K.; Nilsson, S. *J. Colloid Interface Sci.* **1999**, *213*, 152−159.
(46) Kevelam, J.; van Breemen, J. F. L.; Blokzijl, W.; Engberts, J. B. F. N. *Langmuir* **1996**, *12*, 4709−4717.
(47) Soma, J.; Papadopoulos, K. D. *J. Colloid Interface Sci.* **1996**, *181*, 225−231.
(48) Smet, Y. D.; Deriemaeker, L.; Finsy, R. *Langmuir* **1999**, *15*, 6745−6754.
(49) Hoang, T. K. N.; La, V. B.; Deriemaeker, L.; Finsy, R. *Langmuir* **2002**, *18*, 10086−10090.
(50) Chan, H. S.; Dill, K. A. *Proteins: Struct., Funct., Genet.* **1998**, *30*, 2−33.
(51) Matagne, A.; Jamin, M.; Chung, E. W.; Robinson, C. V.; Radford, S. E.; Dobson, C. M. *J. Mol. Biol.* **2000**, *297*, 193−210.
(52) Wallace, M. I.; Ying, L. M.; Balasubramanian, S.; Klenerman, D. *Proc. Natl. Acad. Sci. U.S.A.* **2001**, *98*, 5584−5589.
(53) Collet, O.; Chipot, C. *J. Am. Chem. Soc.* **2003**, *125*, 6573−6580.
(54) Kabalnov, A. S.; Shchukin, E. D. *Adv. Colloid. Interface Sci.* **1992**, *38*, 69−97.

BM060254Y